Characterizing spatiotemporal patterns of air pollution in China: A multiscale landscape approach

Yupeng Liu [a], Jianguo Wu [a,b], Deyong Yu [a,*]

[a] Center for Human-Environment System Sustainability (CHESS), State Key Laboratory of Earth Surface Processes and Resource Ecology (ESPRE), Faculty of Geographical Science, Beijing Normal University, Beijing 100875, China
[b] School of Life Sciences and School of Sustainability, Arizona State University, Tempe, AZ 85287, USA

ABSTRACT

China's tremendous economic growth in the past three decades has resulted in a number of environmental problems, including the deterioration of air quality. In particular, fine particulate matter (PM) has received increasing attention from scientists, governmental agencies, and the public due to its adverse impacts on human health. Monitoring the spatiotemporal patterns of air pollution is important for understanding its transport mechanisms and making effective environmental policies. The main goal of this study, therefore, was to quantify the spatial patterns and movement of air pollution in China at annual, daily, and hourly scales, so that the underlying drivers could be better understood. We used remote sensing data and landscape metrics together to capture spatiotemporal signatures of air pollution. Our results show that, at the annual scale, PM$_{2.5}$ concentrations in China increased gradually from 1999 to 2011, with the highest concentrations occurring in the North China Plain as well as the middle and lower reaches of the Yangtze River Basin. The total population affected by air pollution was about 975 million in 2010 (about 70% of China's population). Our more detailed analysis on daily and hourly scale further revealed that a heavy air pollution event occurred, expanded, aggregated, and finally dissipated over Northern China during Oct. 6–12, 2014, suggesting that the Beijing-Tianjin-Hebei region a center of severe pollution. Crop stalks burning in agricultural areas in this region seemed to be one of the leading drivers, along with coal burning and transportation emissions. Our study demonstrates that spatial pattern analysis with landscape metrics is effective for analyzing source-sink dynamics of air pollution and its potential drivers. Our findings of major source areas and movement trajectories should be useful for making air pollution control policies to improve China's air quality.

© 2017 Elsevier Ltd. All rights reserved.

1. Introduction

China is the most populous country in the world, with more than half of its population now living in cities since 2010 (Liu et al., 2014; Wu et al., 2014). During the past three decades, the concurrent rapid economic growth and urbanization in China are unprecedented in terms of both speed and scale (Ma et al., 2016a; Wu et al., 2014), and have resulted in a number of environmental problems, including the deterioration of air quality in many urban regions across the nation (Huang, 2015; Lue et al., 2010; Shao et al., 2006).

Air pollution can have both acute and chronic effects on human health, ranging from reversible respiratory problems to lung and heart failure-related mortality (Cox, 2013; Folinsbee, 1993; Kampa and Castanas, 2008; Lave and Seskin, 1970; Pant et al., 2016; Phung et al., 2016; Tsangari et al., 2016). For instance, increased air pollution due to fine particulate matter smaller than 2.5 micrometers (PM$_{2.5}$) may lead to the cardiopulmonary morbidity and mortality of people (Lelieveld et al., 2015; Pope and Dockery, 2006; Schwartz et al., 1996; Wu et al., 2014). A recent Chinese case study concluded that the reduction in life expectancy of about 3 years may be expected from long-term exposure to an additional 100 μg/m^3 of Total Suspended Particles (TSPs) (Chen et al., 2013). Especially for elder persons, their relative risks for deaths could be larger than for all ages (Schwartz et al., 1996).

In 2012, the Ministry of Environmental Protection of the People's Republic of China (MEP) updated National Ambient Air Quality Standards, which for the first time included PM$_{2.5}$ (MEP, 2012a).

Table 1
Air Quality Index categories, air pollution levels, and health implications (MEP, 2012b).

AQI	Air pollution level	Health implications
0–50	Excellent	No harm to human health
51–100	Good	Hypersensitive individuals should limit the outdoor activities
101–150	Light Pollution	Children, elder and people with breathing or heart problems should reduce outdoor activities
151–200	Moderate Pollution	Children, elder and people with breathing or heart problems should avoid outdoor exercise
201–300	Heavy Pollution	Children, elder and people with breathing or heart problems should stop outdoor exercise
>300	Severe Pollution	Children, elder and people with breathing or heart problems should stay indoors

Table 2
Air quality standards for specific air pollutants (MEP, 2012b).

IAQI (No unit)	SO_2 ($\mu g/m^3$)	NO_2 ($\mu g/m^3$)	CO (mg/m^3)	O_3 (mg/m^3)	PM_{10} ($\mu g/m^3$)	$PM_{2.5}$ ($\mu g/m^3$)
0	0	0	0	0	0	0
50	50	40	2	100	50	35
100	150	80	4	160	150	75
150	475	180	14	215	250	115
200	800	280	24	265	350	150
300	1600	565	36	800	420	250
400	2100	750	48	–	500	350
500	2620	940	60	–	600	500

Chinese Meteorological Administration (CMA) also updated early-warning standards for air pollution, and expanded the indicator set to include $PM_{2.5}$ concentration, horizontal visibility, and relative humidity (CMA, 2013). The threshold to define and forecast haze days is 75 $\mu g/m^3$ of 24-h mean $PM_{2.5}$ concentration according to the World Health Organization (WHO, 2005). CMA (2013) defined this threshold as 115 $\mu g/m^3$ of 24-h mean $PM_{2.5}$ concentration with relative humidity of higher than 80% and horizontal visibility of less than 3 km, or 150 $\mu g/m^3$ of 24-h mean $PM_{2.5}$ concentration with horizontal visibility of less than 5 km. As per the Chinese standard, the total number of haze days in 2013 was more than 70 in most of China's megacities, including Beijing, Tianjin, Shanghai, Guangzhou, Shenzhen, and a dozen other densely populated urban areas (MEP, 2013). In general, the increase of air pollution in China was a result of human activities such as economic developments (Xu et al., 2016), industrial emissions (Wang et al., 2012a), burning of coal for heating (Tao et al., 2014), and burning of crop stalks (Shi et al., 2014). Rapid urbanization and urban patterns/forms also have impacts on urban air quality (Bereitschaft and Debbage, 2013; Lv and Cao, 2011). Sprawl cities tend to generate more transportation emissions of pollution than more compact cities with mixed land uses (Borrego et al., 2006; Martins, 2012).

To clarify the relationship between air pollution and human health, it is necessary to monitor and quantify the spatiotemporal patterns of air pollution, as well as to understand its transport mechanisms (Blanchard et al., 2011; Yuan et al., 2014; Zhang et al., 2010). Towards this end, observations from air quality monitoring stations are crucial (Cheng et al., 2013; Tao et al., 2014; Wang et al., 2014), but the site-specific measurements must be scaled up to obtain spatial distributional patterns of air pollutants on landscape and regional scales (Pope and Wu, 2014a,b). The accuracy of quantifying air pollution patterns depends on both the density and configuration of the ground stations within a monitoring network, and is also influenced by the scale of analysis in space and time (Pope and Wu, 2014a; Wu, 1999). Air quality monitoring networks provide high temporal resolution data, but their spatial coverage is usually constrained by physical, fiscal, and technical factors (Pope and Wu, 2014b).

To complement the ground-based monitoring data, satellite-based or airborne observations covering broad areas have become increasingly available in recent decades (Tao et al., 2012). Studies have shown that Aerosol Optical Depth (AOD) from satellite observations and $PM_{10}/PM_{2.5}$ concentrations from ground stations are highly correlated (Engel-Cox et al., 2004; Green et al., 2009; Lee et al., 2011; Ma et al., 2016b; van Donkelaar et al., 2006; Wang and Christopher, 2003; Wang et al., 2010b). Based on this correlation, van Donkelaar et al. (2010) and Ma et al. (2016b) derived spatial patterns of annual $PM_{2.5}$ concentrations, indicating that the annual $PM_{2.5}$ concentrations of eastern China exceeded 80 $\mu g/m^3$, which was much higher than the WHO standard of 35 $\mu g/m^3$. In addition to ground and airborne monitoring, remote sensing and Chemical Transport Models (CTMs) have also been used for characterizing the spatiotemporal patterns and simulating the emergence, expansion, and dissipation of the air pollution (Cuchiara et al., 2014; Wang et al., 2012a; Wang et al., 2012b; Wang et al., 2010a; Yahya et al., 2014). For example, such modeling studies have indicated that local emissions (Shi et al., 2014), regional transport (Lue et al., 2010), and secondary aerosol generation (Huang et al., 2014) were the main sources of air pollution, whereas local climate conditions such as high humidity and low wind speed were the key environmental controls (Zhang et al., 2009).

The main objective of this study was two-fold: (i) to quantify the spatial patterns of air pollution on multiple time scales (annual, daily, and hourly) using landscape metrics; and (ii) to identify the potential source and sink regions and drivers of air pollution.

2. Methods

2.1. Data on $PM_{2.5}$

The annual $PM_{2.5}$ concentrations in China were retrieved from the AOD products of MODIS (Moderate Resolution Imaging Spectroradiometer) and MISR (Multiangle Imaging Spectroradiometer) (van Donkelaar et al., 2015). The relationship between total-column AOD and surface dry $PM_{2.5}$ concentrations required a conversion factor which depends on several parameters, including aerosol size, aerosol type, diurnal variation, relative humidity, and the vertical structure of aerosol extinction (van Donkelaar et al., 2010; van Donkelaar et al., 2006). These parameters were obtained through simulations using the GEOS-Chem model (van Donkelaar et al., 2010; van Donkelaar et al., 2006). A three-year running median was used to reduce noise in the annual satellite-derived $PM_{2.5}$ concentration from 1999 to 2011 (van Donkelaar et al., 2015).

2.2. Air quality index

Data on Air Quality Index (AQI) from China's national air quality stations in 161 cities during October 6–12 of 2014 were down-
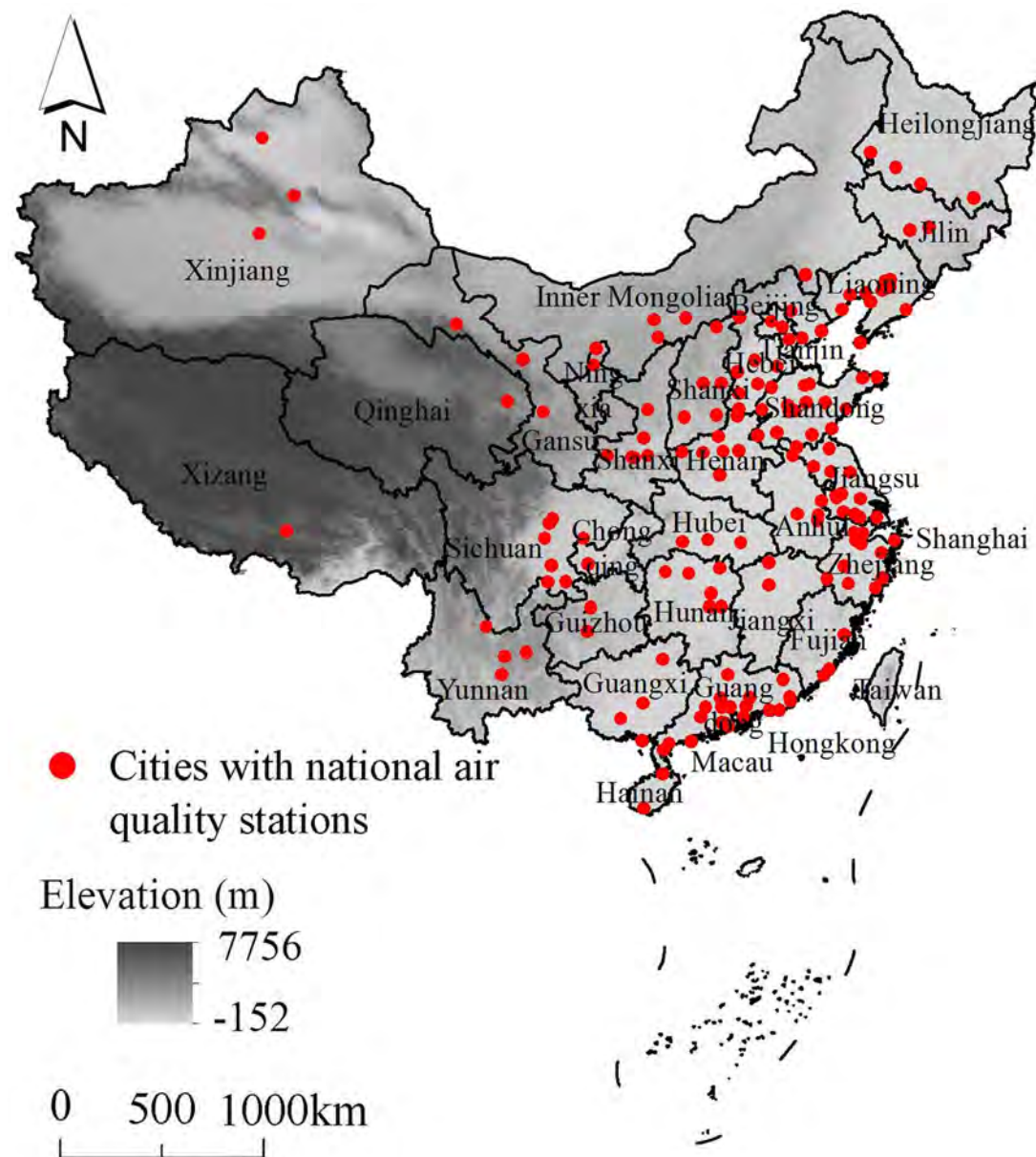
Fig. 1. Spatial distribution of the 161 Chinese cities having national air quality stations in 2014.

loaded from Ministry of Environmental Protection of the People's Republic of China (http://www.zhb.gov.cn/) (Fig. 1) and were interpolated spatially using the ordinary Kriging method with ArcGIS software version 10.0. The AQI indicated the potential health impacts (Table 1). The actual concentrations (C_p) of six air pollutants (SO_2, NO_2, CO, O_3, PM_{10}, and $PM_{2.5}$) were used to calculate AQI (MEP, 2012b):

$$IAQI_n = (IAQI_{Hi} - IAQI_{Lo}) \times \frac{C_p - BP_{Lo}}{BP_{Hi} - BP_{Lo}} + IAQI_{Lo} \qquad (1)$$

$$AQI = \max\{IAQI_1, IAQI_2, IAQI_3, IAQI_4, IAQI_5, IAQI_6\} \qquad (2)$$

where $IAQI_n$ ($n = 1,2,3,...6$) is the individual air quality index for SO_2, NO_2, CO, O_3, PM_{10}, and $PM_{2.5}$, respectively, BP_{Lo} is the break-point concentration at the lower limit of the AQI categories, BP_{Hi} is the break-point concentration at the upper limit of the AQI categories, $IAQI_{Lo}$ is the index value at the lower limit of the AQI categories, and $IAQI_{Hi}$ is the index value at the upper limit of the AQI categories (Table 2). AQI is the maximum value of all $IAQI_n$.

2.3. Quantifying spatial pattern and movement of air pollution

We analyzed the spatial patterns of air pollution on three time scales: the annual, daily, and hourly scales. At the annual scale, we defined an area as "non-polluted" if the annual average $PM_{2.5}$ concentration over it was <35 μg/m³, which was the first interim target of WHO (WHO, 2005) and also the air quality standard used in China (MEP, 2012a). Accordingly, an area with annual average $PM_{2.5}$ concentration of ≥ 35 μg/m³ was considered "polluted". At the daily and hourly scales, AQI <150 was chosen as the threshold value to classify non-polluted and polluted areas (MEP, 2012b).

Landscape pattern metrics have long been used to characterize spatiotemporal dynamics of various kinds of landscapes in ecological and geographical sciences (Buyantuyev et al., 2010; Li et al., 2013a; Li et al., 2013b; Wu et al., 2011). Recently, landscape metrics also have been successfully applied to investigate the relationship between urban patterns/forms and air pollution (Bechle et al., 2011; Bereitschaft and Debbage, 2013; Borrego et al., 2006; Lv and Cao, 2011). In this study, we selected five class-level landscape

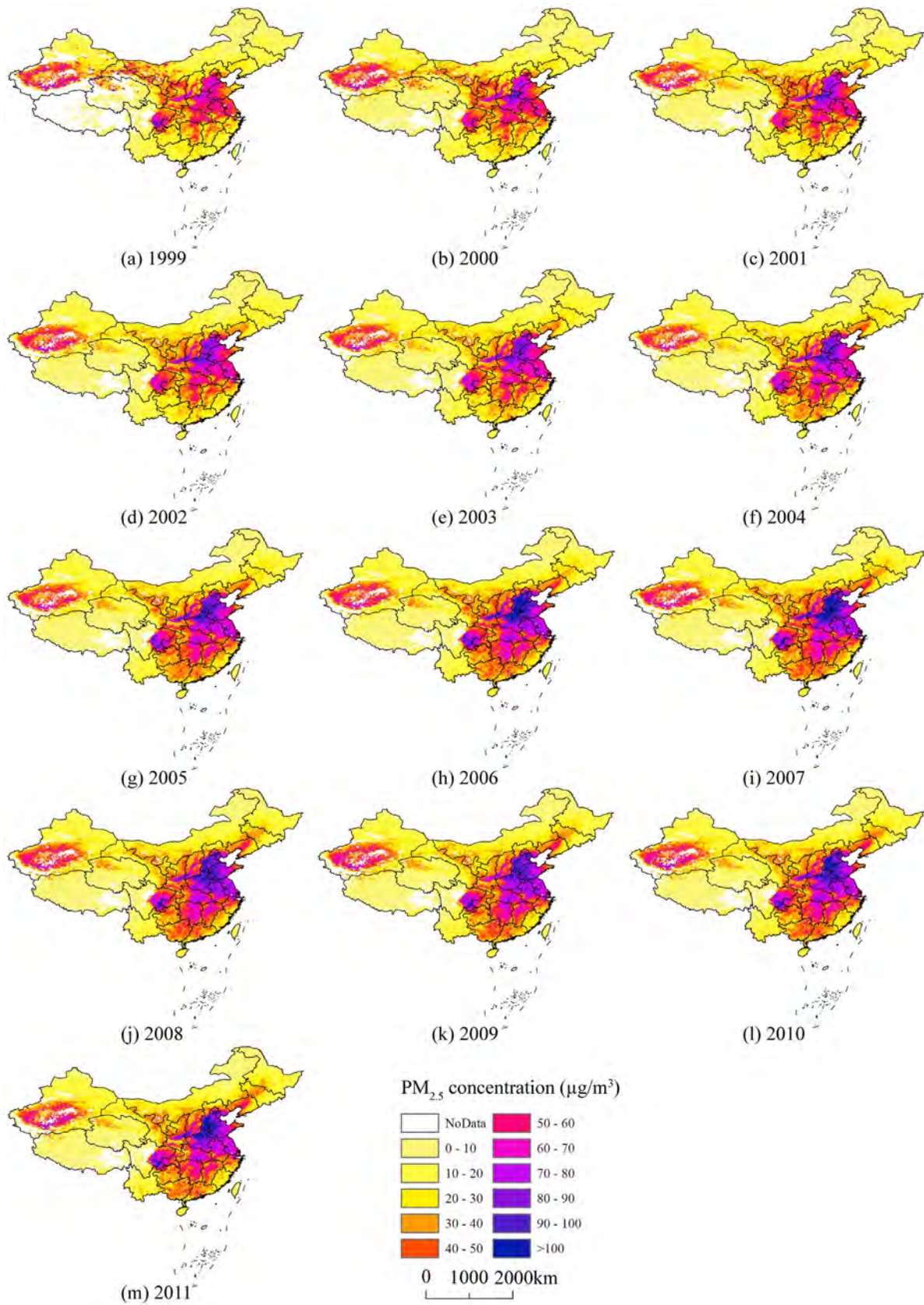**Fig. 2.** Spatial patterns of annual PM$_{2.5}$ concentrations (μg/m^3) in China from 1999 to 2011. We created these maps with ARCGIS 10.0 software. Original PM$_{2.5}$ concentration data were from van Donkelaar et al., 2015 and spatial resolution was 0.1°.
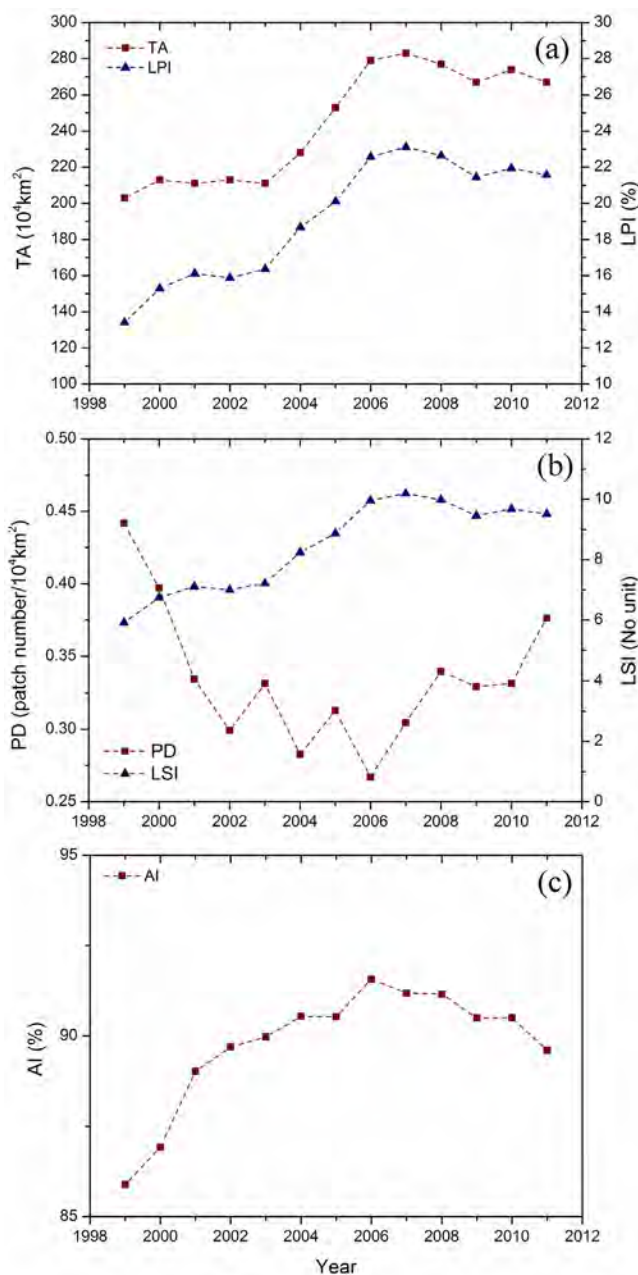
Fig. 3. Spatiotemporal patterns of air-polluted areas (annual average $PM_{2.5}$ concentration >35 μg/m^3) in China as described by five class-level pattern metrics.

metrics to quantify the spatial distribution patterns of air pollutants because of their effectiveness for characterizing the spatial extent, aggregation, and interspersion of landscape elements from previous studies of urbanization impacts on environmental conditions, such as biodiversity, net primary productivity, and urban heat islands (Buyantuyev and Wu, 2010; Buyantuyev et al., 2010; Li et al., 2013a; Li et al., 2013b; Wu, 2004; Wu et al., 2011; Wu et al., 2002). They are: Total Area (TA), Largest Patch Index (LPI), Patch Density (PD), Landscape Shape Index (LPI), and Aggregation Index (AI) (Table A.1). Total Area is simply the sum total of all air-polluted patches, where a "patch" is a contiguous air-polluted area. Largest Patch Index is the area of the largest polluted patch relative to the whole study area (i.e., China). Patch Density is the number of patches per unit area, suggestive of the degree of fragmentation or interspersion of polluted areas. Landscape Shape Index is a normalized perimeter/area ratio of patches, a measure of the shape complexity of air-polluted patches. Aggregation Index (He

et al., 2000) measures the degree of aggregation or clumping of polluted patches and considers only the adjacencies between polluted patches. All the selected metrics were computed with the FRAGSTATS software (v4.2) (McGarigal et al., 2012).

Two methods were used to determine the movement of air-polluted areas beyond pattern analysis. One was tracing the geometric center of the largest air pollution patch (AQI >200 or 150) in a specific air pollution event using the ARCGIS 10.0 software. The other was simulating the transport of air masses using a process-based HYSPLIT (Hybrid Single-Particle Lagrangian Integrated Trajectory) model (Rolph, 2016; Stein et al., 2015).

3. Results

3.1. Spatiotemporal patterns of air pollution on the annual scale

From 1999–2011, annual $PM_{2.5}$ concentrations in China generally increased in both spatial extent and intensity (Fig. 2). High
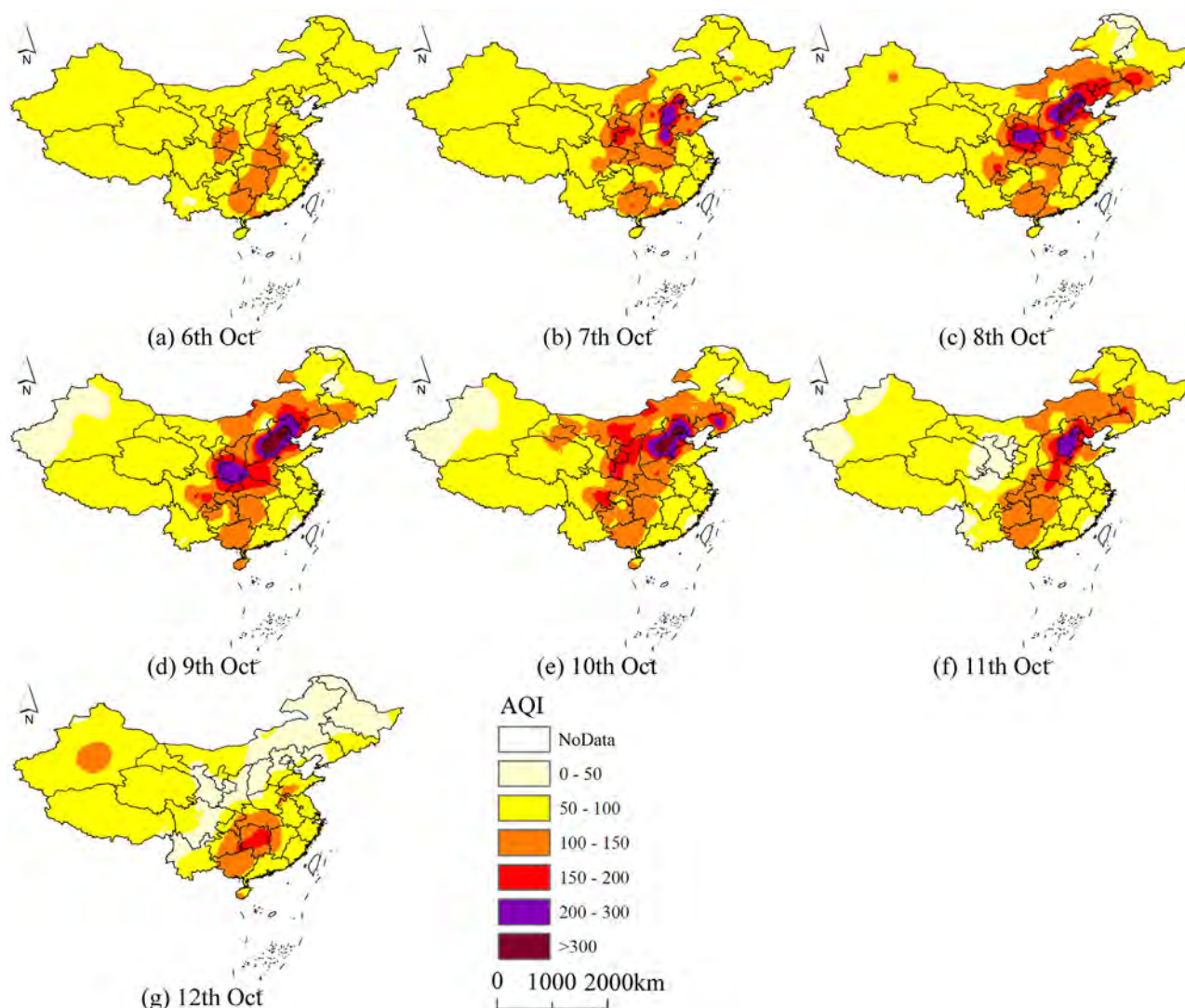
Fig. 4. Temporal changes in the spatial pattern of daily AQI in China during Oct. 6–12, 2014, highlighting the emergence-coalescence-dissipation process of a severe air pollution event (AQI > 150) that occurred in the North China Plain from Oct. 7 to Oct. 11, 2014.

concentrations of PM$_{2.5}$ occurred over a vast region of China, ranging from southern Inner Mongolia to Guangdong latitudinally, and from the east coast to central Sichuan longitudinally, plus the southern part of Xinjiang Province (Fig. 2). In particular, the highest concentrations occurred in the North China Plain (Beijing, Tianjin, Hebei, Shandong, Henan, northern Jiangsu, and northern Anhui) and the middle and lower reaches of the Yangtze River Basin (Fig. 2).

The air-polluted areas (i.e., places with annual average PM$_{2.5}$ concentrations of higher than 35 μg/m^3) increased rapidly from about 2 million km^2 in 1999 to about 2.8 million km^2 in 2006, and then began to decline slightly after 2006 (Fig. 3a). The total population living within the air-polluted areas was about 975 million in 2010 (about 70% of China's population; population data derived from LandScan 2010 dataset (Bright et al., 2011)). The largest contiguous region of air pollution occurred over the North China Plain and the middle and lower reaches of the Yangtze River Basin, accounting for 14% of China's total land area in 1999 and 22% in 2011 (Fig. 3a). Landscape Shape Index exhibited a quite similar temporal pattern to that of total air polluted areas (Fig. 3b). Patch Density of air polluted areas decreased from 1999 to 2006, and then increased rapidly from 2006 to 2011 (Fig. 3b). Aggregation Index increased first, peaking in 2006, and then began to decline (Fig. 3c).

3.2. Spatiotemporal patterns of air pollution on the daily scale

To understand the spatial patterns of air pollution on finer temporal scales, we also examined a regional air pollution event (AQI >150) that emerged, expanded, and then dissipated in the North China Plain during Oct. 6–12, 2014 (Fig. 4). Changes in the spatial pattern metrics indicated some key attributes of the spatial dynamics of this event. Total Area, Largest Patch Index, Landscape Shape Index, and Aggregation Index of air-polluted areas all increased from Oct. 7 to Oct. 9, and then decreased from Oct. 9 to Oct. 12 (Fig. 5a to c). Patch Density of air polluted areas increased initially from Oct. 7 to Oct. 8, and then decreased rapidly from Oct. 9 to Oct. 12 (Fig. 5b).

3.3. Spatiotemporal patterns of air pollution on the hourly scale

At the hourly scale, more details were revealed about the spatiotemporal pattern of the regional air pollution event in the North China Plain during Oct. 6–12, 2014: the pollution occurred and expanded from 21:00 of Oct. 6–00:00 of Oct. 8 (Fig. 6a to k), sustained from 00:00 of Oct. 8–15:00 of Oct. 11, finally weakened and dissipated from 15:00 of Oct. 11–12:00 of Oct. 12 (Fig. 6l to s). During this period, Total Area, Largest Patch Index, Landscape Shape
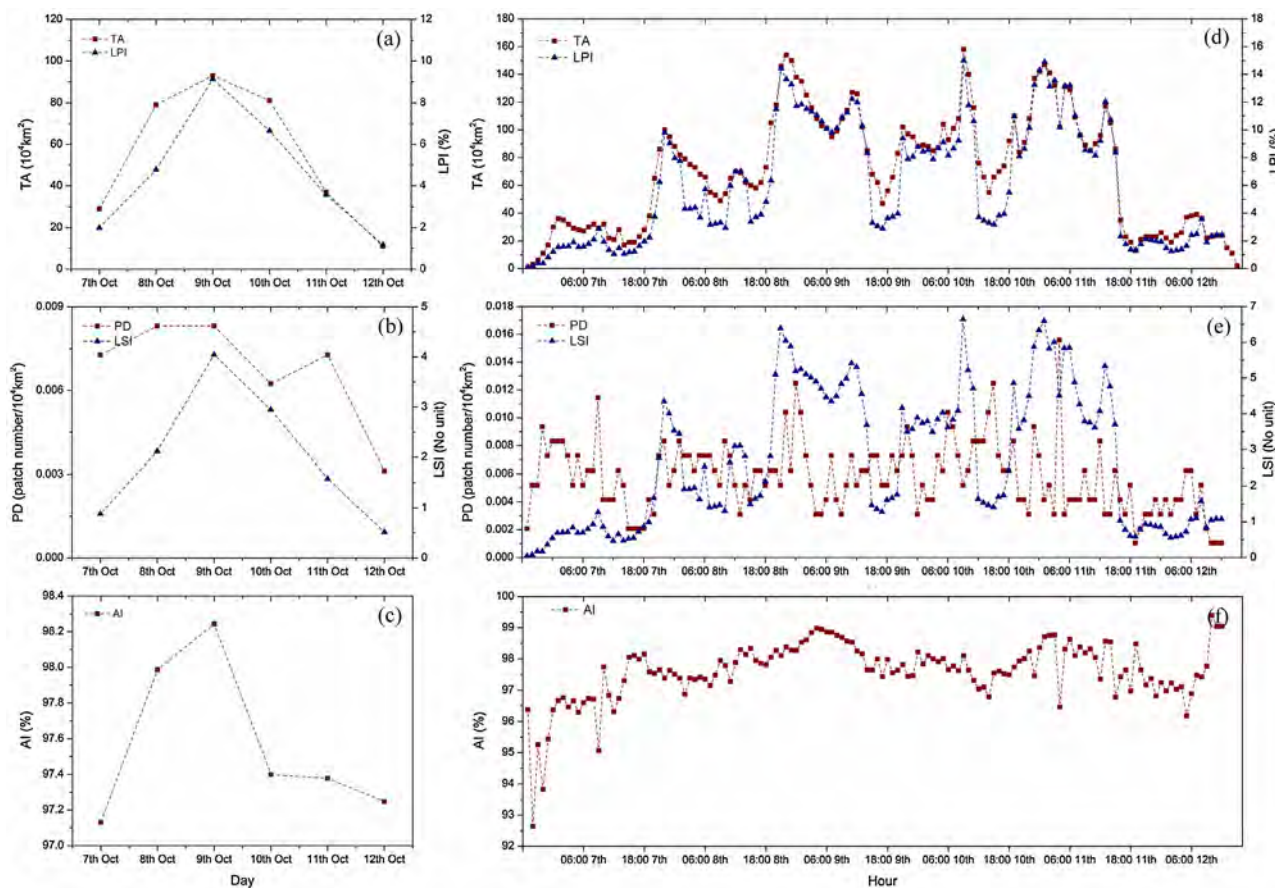
Fig. 5. Spatiotemporal patterns of air-polluted areas in China during Oct. 7–12, 2014 as described by five class-level pattern metrics. Daily patterns were shown in (a)–(c), corresponding to the maps in Fig. 4, and hourly patterns were illustrated in (d)–(f), corresponding to the maps in Fig. 6.

Index, and Aggregation Index of air-polluted areas generally peaked during nighttime and slightly decreased during daytime (Fig. 5d to f).

The geometric center of the largest air-polluted patch was at the junction of the Hebei, Henan, and Shandong Province on Oct. 7, moved northward and sustained mostly in Beijing-Tianjin-Hebei region during Oct. 7–11, and then moved southward and dissipated in Shandong Province on Oct. 12 (Fig. 7). The trajectories under more rigid criteria (AQI >200 than 150) indicated that the Beijing-Tianjin-Hebei region was the center of severe pollution (Fig. 7). The simulated trajectories of air masses with HYSPLIT model were also shown that air pollutants could move northward from Henan and Shandong Province to Beijing, Tianjin, and Shijiazhuang during Oct. 7 and Oct. 8, 2014 (Fig. 8). Several locations of burning crop stalks were identified from the daily reports of the Chinese Ministry of Environmental Protection, most of which were adjacent to the trajectories of air masses (Fig. 8).

4. Discussion

4.1. Quantifying spatiotemporal patterns of air pollution on broad scales

The results of our analysis with landscape metrics clearly indicated that air-polluted areas in China expanded rapidly during our study period (1999–2011), with the highest increase rate occurring between 1999 and 2006 (Fig. 3a). The unprecedented scale of urbanization, rapid economic growth, and increasing energy use took place on currently with the deterioration of air pollution (Fritze, 2004; Wu et al., 2014). An increase in Aggregation Index

and a decrease in Patch Density from 1999 to 2006 indicated that many scattered air-polluted areas merged into fewer, larger and more clumped patches, hanging mainly over the North China Plain, the middle and lower reaches of the Yangtze River Basin, the Pearl River Delta, and the Sichuan Basin. These regions include Beijing, Tianjin, Zhengzhou, Shanghai, Guangzhou, Chengdu and a dozen other densely populated megacities.

A decrease in Aggregation Index and an increase in Patch Density from 2006 to 2011 resulted from previously clumped air-polluted patches splitting into smaller pieces. The slight decreases in Total Area, Largest Patch Index, and Landscape Shape Index of air-polluted areas suggested a slowdown or even a halt of the deterioration of air pollution during this period. According to the Statistical Yearbook of China (http://www.stats.gov.cn/tjsj/ndsj/), the country's annual emissions of SO_2 and PM peaked in 2006 and 2005, respectively, and then started to decline. A main reason for this temporary air quality improvement might have been the implementation of flue-gas desulfurization in electricity-generating plants required by the Chinese government, leading to substantial reductions of SO_2 (a precursor of $PM_{2.5}$) emissions since 2006 (Li et al., 2010). In addition, the efficiency improvement in central heating systems in Chinese cities also reduced the urban household energy consumptions and $PM_{2.5}$ emissions (Guan et al., 2014).

4.2. Quantifying spatiotemporal patterns of air pollution on fine scales

Using Largest Patch Index, we were able to identify that the largest contiguous air-polluted patch with high $PM_{2.5}$ concentra-

tion occurred in the North China Plain (Fig. 3a). To understand this heavily polluted region in greater detail, we further analyzed the spatial dynamics of a regional air pollution event on finer temporal scales. The five landscape metrics together captured the entire process of the event: from emergence to expansion and dissipation. Total Area, Largest Patch Index, Landscape Shape Index, and Aggregation Index all increased first, then peaked at different times, and finally decreased, exhibiting a unimodal pattern. Patch Density was low at both the beginning and the end of the severe air pollution

event, and reached its highest value in between, thus exhibiting a bimodal pattern (Fig. 5b).

Compared to those at the daily scale, the changing patterns of Total Area, Largest Patch Index, Landscape Shape Index, and Aggregation Index at the hourly scale peaked mostly during nighttime and decreased slightly during daytime. This diurnal pattern can be explained largely by micrometeorological changes induced by land-atmospheric interactions. At sunset, the ground surface cools faster than the atmosphere, which often leads to the inversion of the normal vertical temperature gradient at low altitudes in the lower
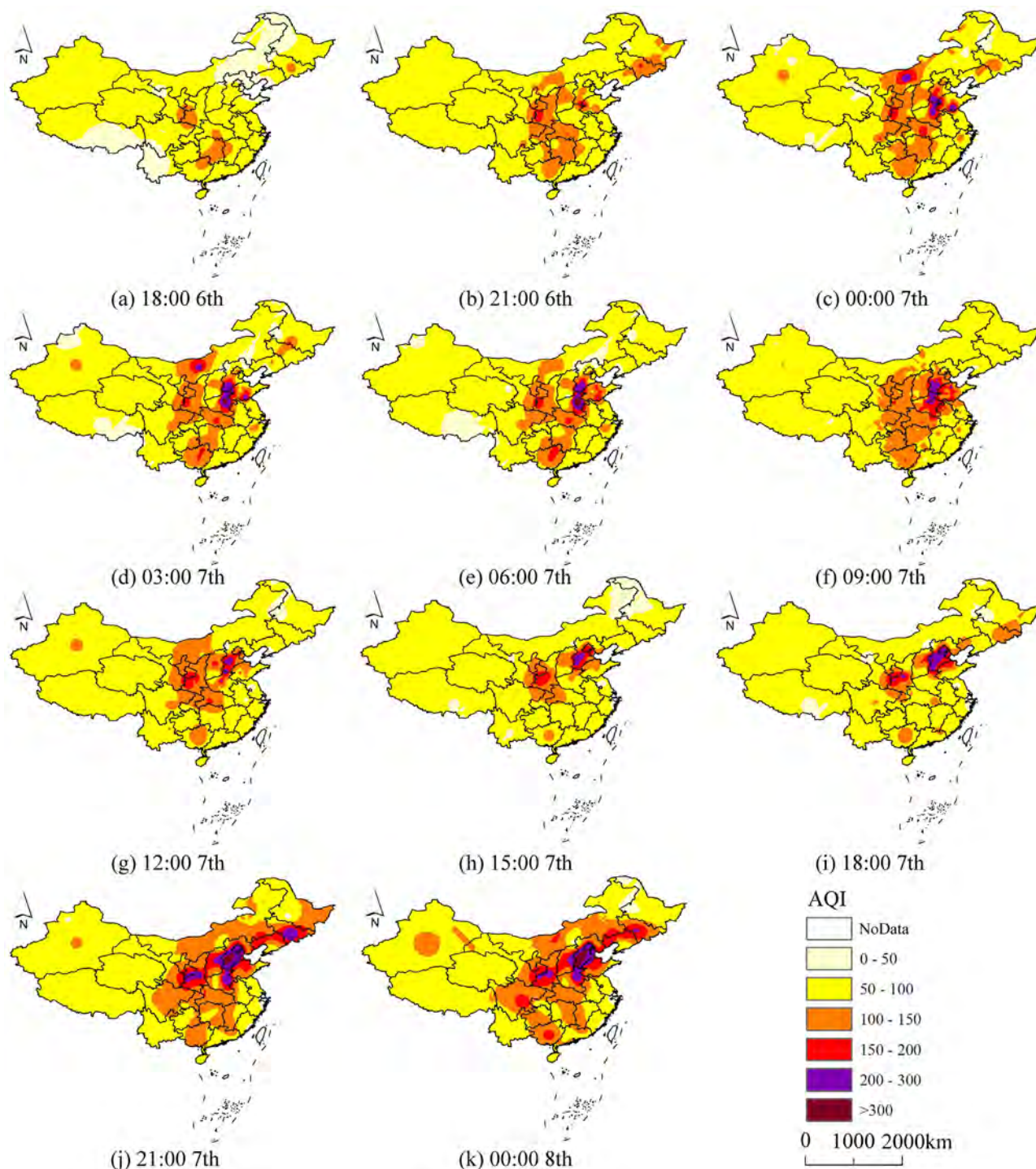

Fig. 6. Temporal changes in the spatial pattern of hourly AQI in China, showing that the severe air pollution event occurred and expanded in the North China Plain between 21:00 of Oct. 6 and 00:00 of Oct. 8 (a–k), and then weakened and dissipated between 15:00 of Oct. 11 and 12:00 of Oct. 12, 2014 (l–s).
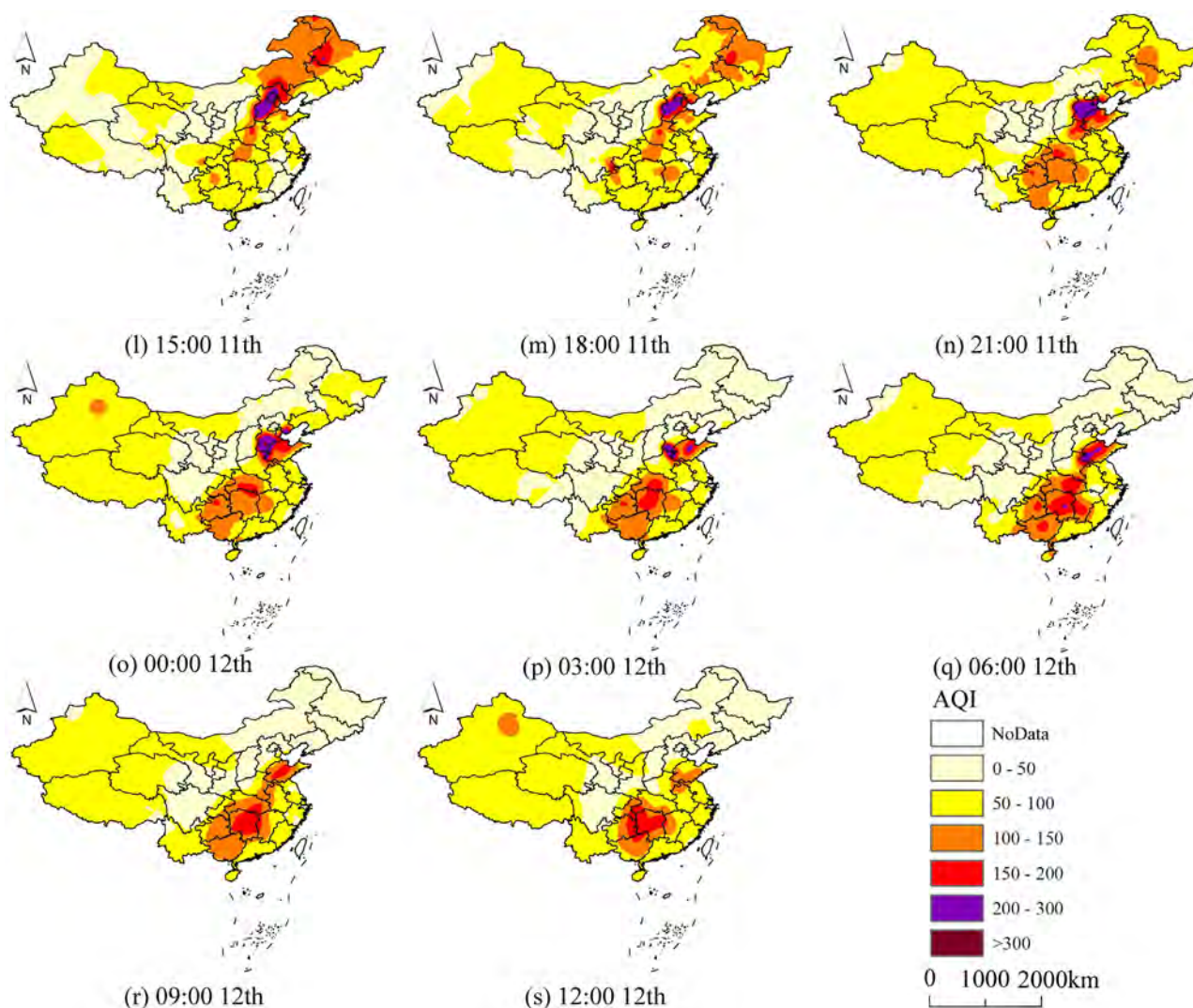
(l) 15:00 11th   (m) 18:00 11th   (n) 21:00 11th

(o) 00:00 12th   (p) 03:00 12th   (q) 06:00 12th

AQI

☐ NoData
☐ 0 - 50
☐ 50 - 100
☐ 100 - 150
☐ 150 - 200
☐ 200 - 300
☐ >300

0   1000 2000km

(r) 09:00 12th   (s) 12:00 12th

Fig. 6. (Continued)

atmosphere (a.k.a., temperature inversion), thus hindering the dissipation of air pollution upward during nighttime (Pardyjak et al., 2009; Pope and Wu, 2014a). While this emergence-coalescence-dissipation pattern of a heavy air pollution event is can be readily perceived, quantifying it in space and time with landscape metrics improves the precision of our understanding and helps impact assessment and policy-making with regard to air pollution.

4.3. Identifying source and sink areas of air pollution

By computing the geometric center and tracing the movement trajectory of air pollution, we were able to identify the potential source and sink areas for a severe air pollution event in China during October of 2014. Specifically, the air pollution center was formed in Henan Province, western Shandong Province, and southern Hebei Province on Oct. 7, 2014 (Fig. 7), indicative of this region as potential source area. During Oct. 8–11, 2014, the center of this heavy pollution (AQI >200) moved to the Beijing-Tianjin-Hebei region, and then it moved southward to eastern Shandong Province, and dissipated by northwest wind finally, indicating that eastern Shandong Province was a sink area for this particular event.

The North China Plain was a densely populated and highly urbanized region with the highest frequency of haze events during the past several decades (Hu and Zhou, 2009; Wang et al., 2012a).

Our study suggests that burning of crop stalks in Hebei Province, Henan Province and Shandong Province may be one of the potential leading factors, in addition to industrial and motor vehicle emissions, for generating regional air pollution events. PM$_{2.5}$ and other kinds of air pollutants from burning crop stalks maybe transported by southerly wind to the Beijing-Tianjin-Hebei region (Fig. 8). PM$_{2.5}$ is both a primary and secondary pollutant, which can be emitted directly from vehicle exhaust, agricultural biomass burning, and industrial plants, or formed from Secondary Organic Aerosols (SOA) and Secondary Inorganic Aerosols (SIA) (Beijing Municipal Environmental Protection Bureau, 2014; Huang et al., 2014). These sources have also been found important within the Beijing-Tianjin-Hebei region (Huang et al., 2014). In addition, reduced wind speed and high relative humidity in this region are two key environmental factors hindering pollution dissipation (Tao et al., 2014; Wang et al., 2012a).

4.4. Robustness of the results and future directions

Dense air quality monitoring stations in eastern China provide enough samples for reliable interpolation of AQI values within this region. However, air quality monitoring stations in western China are sparse, resulting in less accurate interpolated values of AQI. In particular, the interpolated AQI values for the provinces of Xinjiang,
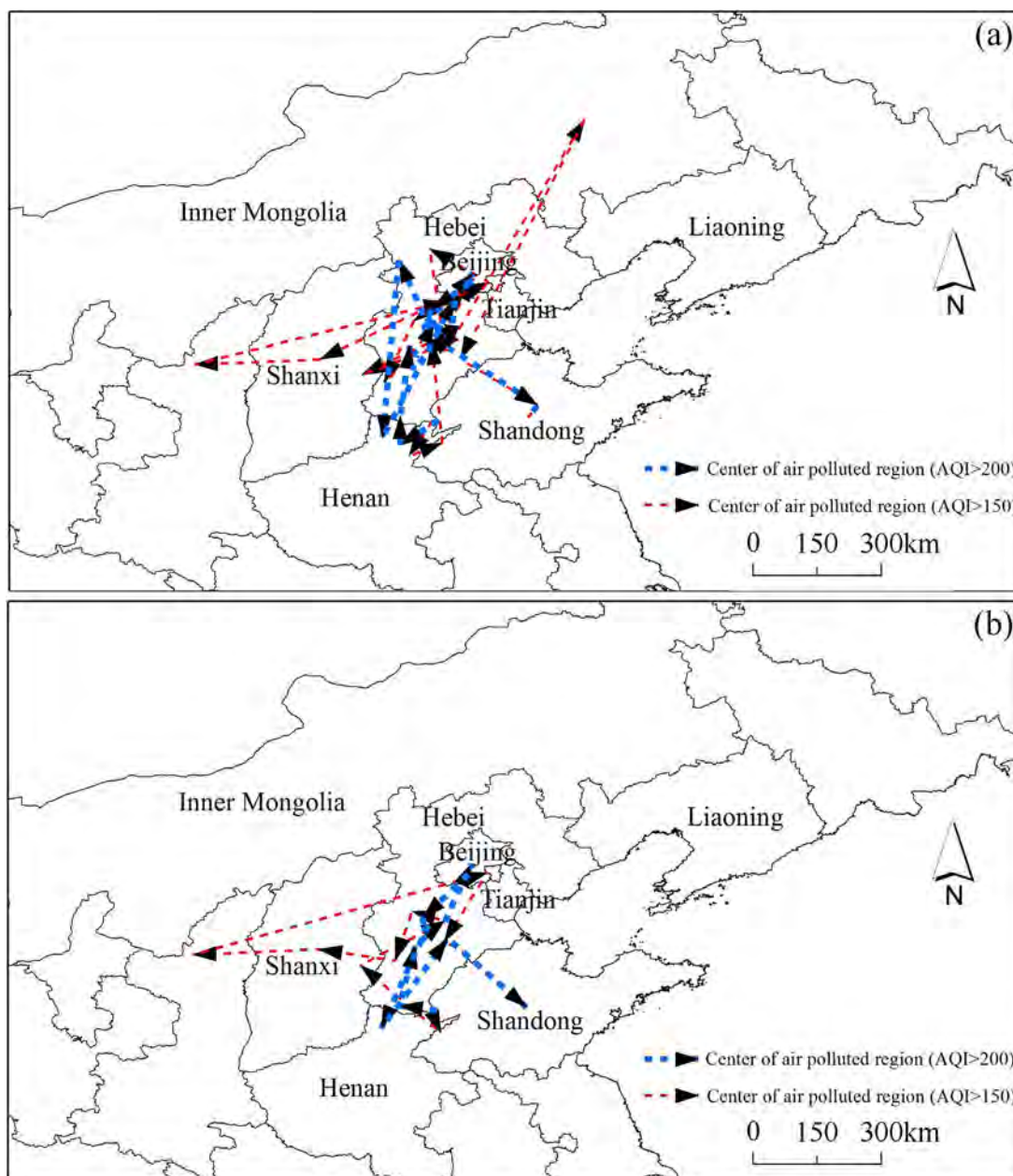
Fig. 7. The geometric center and trajectory of the largest air pollution patch (hourly AQI > 150 as thinner dashed lines and AQI > 200 as thicker dashed lines) in the North China Plain between 21:00 of Oct. 6 and 12:00 of Oct. 12, 2014. The trajectory in (a) was drawn per 6 h, and the one in (b) was per 12 h. The geometric center and trajectory were calculated and drawn with ARCGIS 10.0 software.

Tibet, Qinghai, Gansu, and western Sichuan in Figs. 4 and 6 have relatively high uncertainties. Nevertheless, the general spatiotemporal patterns of air pollution revealed in our study are robust because numerous studies have documented that severe air pollution events during the recent decades took place mainly in eastern China.

To improve the accuracy of air pollution assessment at the national level, however, more air quality monitoring stations are needed in western China, which should be designed based on local air pollutants and environmental conditions (Pope and Wu, 2014a,b). In addition, broad-scale analyses based on remote sensing data, such as our study here, should be integrated with fine-scale site measurements to better understand the processes and mechanisms of the source-sink dynamics of air pollution in China.

5. Conclusions

Using remote sensing data, field-based monitoring data, and landscape metrics, we were able to quantify the spatiotemporal patterns of air pollution on multiple scales in China. Our results indicate that the total area, intensity, aggregation, and shape complexity of air-polluted areas increased substantially across China during the study period. The most severely air-polluted area was the North China Plain, within which the Beijing-Tianjin-Hebei region was the worst. By quantifying the patch dynamics of air pollution and keeping track of the movement of pollution centers, we were also able to identify source and sink areas. We estimated that the total population affected by air pollution in China during 2010 was about 975 million, accounting for almost 70% of China's population. Because long-term exposure to high concentrations of air
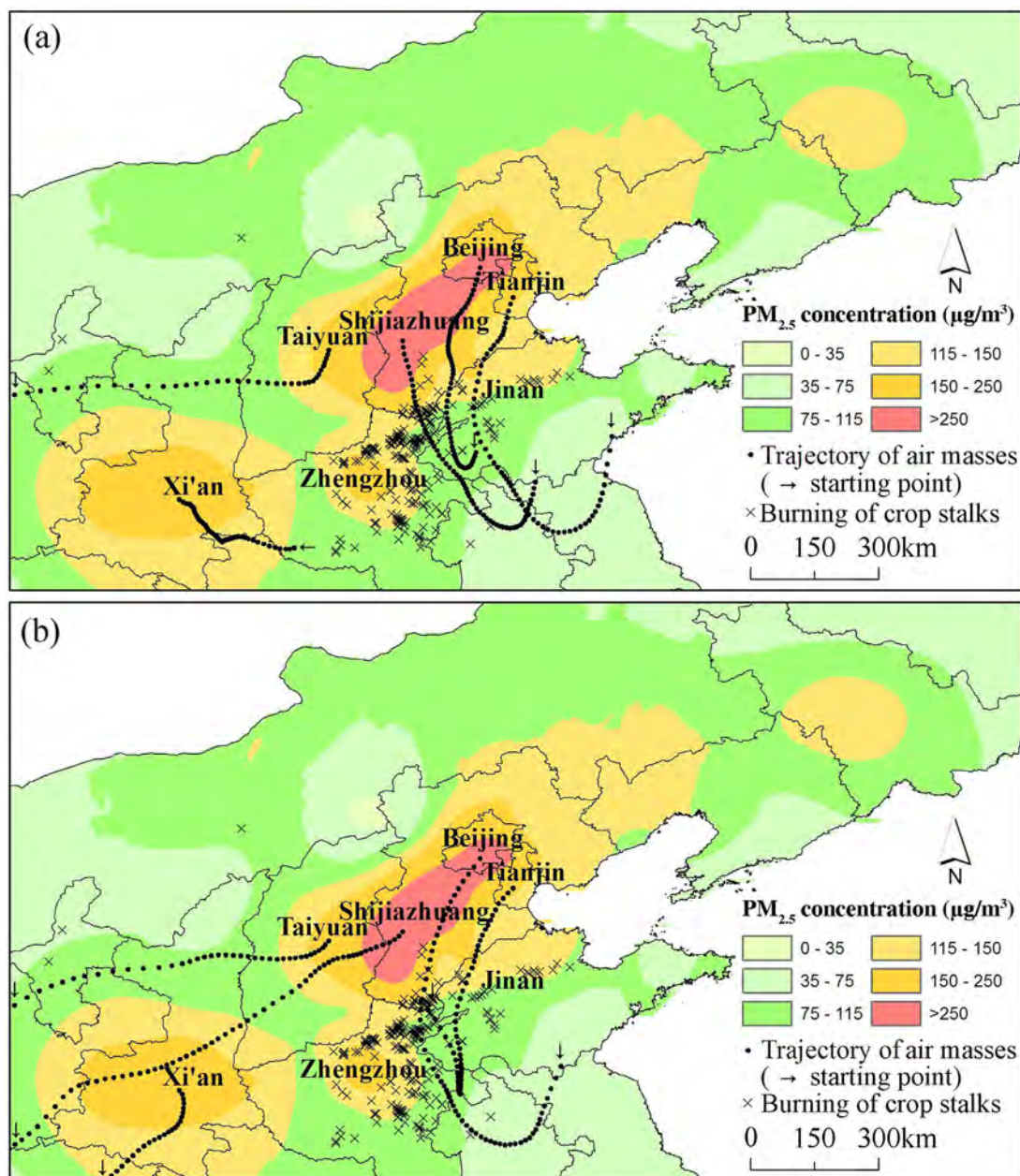
Fig. 8. Spatial patterns of PM$_{2.5}$ concentrations and 60-h backward trajectories of air masses moving through Beijing, Tianjin, Shijiazhuang, Taiyuan, and Xi'an from 00:00 of Oct. 6–12:00 of Oct. 8, 2014. Trajectories of air masses at the altitudes of 500 m (a) and 1000 m (b) were shown. Crosses denoted the sites of burning crop stalks which were detected by satellite (data from http://www.zhb.gov.cn/). The trajectories of air masses were simulated by HYSPLIT model (Rolph, 2016; Stein et al., 2015).

pollutants has serious detrimental impacts on human health, China needs to take immediate and drastic measures to improve its air quality. Towards this end, the results of our study should be useful for designing effective policies to control air pollution on regional and national levels by explicitly recognizing major source areas and movement trajectories.

Appendix A. Supplementary data

Supplementary data associated with this article can be found, in the online version, at http://dx.doi.org/10.1016/j.ecolind.2017.01.027.

References

Bechle, M.J., Millet, D.B., Marshall, J.D., 2011. Effects of income and urban form on urban NO2: global evidence from satellites. Environ. Sci. Technol. 45, 4914–4919, http://dx.doi.org/10.1021/es103866b.

Beijing Municipal Environmental Protection Bureau (BJEPB), 2014. Source analysis of PM2.5 in Beijing, Beijing. Retrieved from – http://www.bjepb.gov.cn/bjepb/323265/340674/396253/index.html.

Bereitschaft, B., Debbage, K., 2013. Urban form, air pollution, and CO2 emissions in large U.S. metropolitan areas. Prof. Geogr. 65, 612–635, http://dx.doi.org/10.1080/00330124.2013.799991.

Blanchard, C.L., Tanenbaum, S., Motallebi, N., 2011. Spatial and temporal characterization of PM2.5 mass concentrations in california, 1980–2007. J. Air Waste Manage. Assoc. 61, 339–351, http://dx.doi.org/10.3155/1047-3289.61.3.339.

Borrego, C., Martins, H., Tchepel, O., Salmim, L., Monteiro, A., Miranda, A.I., 2006. How urban structure can affect city sustainability from an air quality perspective. Environ. Model. Softw. 21, 461–467, http://dx.doi.org/10.1016/j.envsoft.2004.07.009.

Bright, E.A., Coleman, P.R., Rose, A.N., Urban, M.L., 2011. LandScan 2010, 2010 ed. Oak Ridge National Laboratory, Oak Ridge, TN.

Buyantuyev, A., Wu, J., 2010. Urban heat islands and landscape heterogeneity: linking spatiotemporal variations in surface temperatures to land-cover and socioeconomic patterns. Landsc. Ecol. 25, 17–33, http://dx.doi.org/10.1007/s10980-009-9402-4.

Buyantuyev, A., Wu, J., Gries, C., 2010. Multiscale analysis of the urbanization pattern of the Phoenix metropolitan landscape of USA: time, space and thematic resolution. Landsc. Urban Plan. 94, 206–217, http://dx.doi.org/10.1016/j.landurbplan.2009.10.005.

2013. Revised Standard of Haze Warning Singles (on Trial). China Meteorological News Press, Beijing.

Chen, Y., Ebenstein, A., Greenstone, M., Li, H., 2013. Evidence on the impact of sustained exposure to air pollution on life expectancy from China's Huai River policy. Proc. Natl. Acad. Sci. U. S. A. 110, 12936–12941, http://dx.doi.org/10.1073/pnas.1300018110.

Cheng, Z., Wang, S., Jiang, J., Fu, Q., Chen, C., Xu, B., Yu, J., Fu, X., Hao, J., 2013. Long-term trend of haze pollution and impact of particulate matter in the Yangtze River Delta, China. Environ. Pollut. 182, 101–110, http://dx.doi.org/10.1016/j.envpol.2013.06.043.

Cox, L.A., 2013. Caveats for causal interpretations of linear regression coefficients for fine particulate (PM2.5) air pollution health effects. Risk Anal. 33, 2111–2125, http://dx.doi.org/10.1111/risa.12084.

Cuchiara, G.C., Li, X., Carvalho, J., Rappenglück, B., 2014. Intercomparison of planetary boundary layer parameterization and its impacts on surface ozone concentration in the WRF/Chem model for a case study in Houston/Texas. Atmos. Environ. 96, 175–185, http://dx.doi.org/10.1016/j.atmosenv.2014.07.013.

Engel-Cox, J.A., Holloman, C.H., Coutant, B.W., Hoff, R.M., 2004. Qualitative and quantitative evaluation of MODIS satellite sensor data for regional and urban scale air quality. Atmos. Environ. 38, 2495–2509, http://dx.doi.org/10.1016/j.atmosenv.2004.01.039.

Folinsbee, L.J., 1993. Human health effects of air pollution. Environ. Health. Persp. 100, 45–56, http://dx.doi.org/10.1289/ehp.9310045.

Fritze, 2004. Urbanization, Energy, and Air Pollution in China, Urbanization, Energy, and Air Pollution in China. The national academies press, Washinton, D.C, p. 1.

Green, M., Kondragunta, S., Ciren, P., Xu, C., 2009. Comparison of GOES and MODIS aerosol optical depth (AOD) to aerosol robotic network (AERONET) AOD and IMPROVE PM2.5 mass at bondville, illinois. J. Air Waste Manage. Assoc. 59, 1082–1091, http://dx.doi.org/10.3155/1047-3289.59.9.1082.

Guan, D., Su, X., Zhang, Q., Peters, P.G., Liu, Z., Lei, Y., He, K., 2014. The socioeconomic drivers of China's primary PM 2.5 emissions. Environ. Res. Lett. 9, 024010, http://dx.doi.org/10.1088/1748-9326/9/2/024010.

He, H., DeZonia, B., Mladenoff, D., 2000. An aggregation index (AI) to quantify spatial patterns of landscapes. Landsc. Ecol. 15, 591–601, http://dx.doi.org/10.1023/a:1008102521322.

Hu, Y., Zhou, C., 2009. Climatic characteristics of haze in China. Meteorol. Mon. (in Chinese) 35, 73–78.

Huang, R., Zhang, Y., Bozzetti, C., Ho, K., Cao, J., Han, Y., Daellenbach, K.R., Slowik, J.G., Platt, S.M., Canonaco, F., Zotter, P., Wolf, R., Pieber, S.M., Bruns, E.A., Crippa, M., Ciarelli, G., Piazzalunga, A., Schwikowski, M., Abbaszade, G., Schnelle-Kreis, J., Zimmermann, R., An, Z., Szidat, S., Baltensperger, U., Haddad, I.E., Prevot, A.S.H., 2014. High secondary aerosol contribution to particulate pollution during haze events in China. Nature 514, 218–222, http://dx.doi.org/10.1038/nature13774.

Huang, G., 2015. PM2.5 opened a door to public participation addressing environmental challenges in China. Environ. Pollut. 197, 313–315, http://dx.doi.org/10.1016/j.envpol.2014.12.001.

Kampa, M., Castanas, E., 2008. Human health effects of air pollution. Environ. Pollut. 151, 362–367, http://dx.doi.org/10.1016/j.envpol.2007.06.012.

Lave, L.B., Seskin, E.P., 1970. Air pollution and human health. Science 169, 723–733.

Lee, H.J., Liu, Y., Coull, B.A., Schwartz, J., Koutrakis, P., 2011. A novel calibration approach of MODIS AOD data to predict PM2.5 concentrations. Atmos. Chem. Phys. 11, 7991–8002, http://dx.doi.org/10.5194/acp-11-7991-2011.

Lelieveld, J., Evans, J.S., Fnais, M., Giannadaki, D., Pozzer, A., 2015. The contribution of outdoor air pollution sources to premature mortality on a global scale. Nature 525, 367–371, http://dx.doi.org/10.1038/nature15371.

Li, C., Zhang, Q., Krotkov, N.A., Streets, D.G., He, K., Tsay, S.C., Gleason, J.F., 2010. Recent large reduction in sulfur dioxide emissions from Chinese power plants observed by the ozone monitoring instrument. Geogr. Res. Lett. 37, 292–305, http://dx.doi.org/10.1029/2010gl042594.

Li, C., Li, J., Wu, J., 2013a. Quantifying the speed, growth modes, and landscape pattern changes of urbanization: a hierarchical patch dynamics approach. Landsc. Ecol. 28, 1875–1888, http://dx.doi.org/10.1007/s10980-013-9933-6.

Li, J., Li, C., Zhu, F., Song, C., Wu, J., 2013b. Spatiotemporal pattern of urbanization in Shanghai, China between 1989 and 2005. Landsc. Ecol. 28, 1545–1565, http://dx.doi.org/10.1007/s10980-013-9901-1.

Liu, Z., He, C., Zhou, Y., Wu, J., 2014. How much of the world's land has been urbanized, really? A hierarchical framework for avoiding confusion. Landsc. Ecol. 29, 763–771, http://dx.doi.org/10.1007/s10980-014-0034-y.

Lue, Y., Liu, L.Y., Hu, X., Wang, L., Guo, L.L., Gao, S.Y., Zhang, X.X., Tang, Y., Qu, Z.Q., Cao, H.W., Jia, Z.J., Xu, H.Y., Yang, Y.Y., 2010. Characteristics and provenance of dustfall during an unusual floating dust event. Atmos. Environ. 44, 3477–3484, http://dx.doi.org/10.1016/j.atmosenv.2010.06.027.

Lv, B., Cao, N., 2011. Environmental performance evaluation of chinese urban form. Urban Stud. (in Chinese) 18, 38–47.

Ministry of Environmental Protection of the People's Republic of China (MEP), 2012a. Ambient Air Quality Standards. China Environmental Science Press, Beijing.

Ministry of Environmental Protection of the People's Republic of China (MEP), 2012b. Technical Regulation on Ambient Air Quality Index (on Trial), HJ 633–2012. China Environmental Science Press, Beijing.

Ministry of Environmental Protection of the People's Republic of China (MEP), 2013. Analysis Report on the State of the Environment in China, 2013, Beijing.

Ma, Q., Wu, J., He, C., 2016a. A hierarchical analysis of the relationship between urban impervious surfaces and land surface temperatures: spatial scale dependence, temporal variations, and bioclimatic modulation. Landsc. Ecol. 31, 1139–1153, http://dx.doi.org/10.1007/s10980-016-0356-z.

Ma, Z., Hu, X., Sayer, A.M., Levy, R., Zhang, Q., Xue, Y., Tong, S., Bi, J., Huang, L., Liu, Y., 2016b. Satellite-based spatiotemporal trends in PM2.5 concentrations: China, 2004–2013. Environ. Health. Persp. 124, 184–192, http://dx.doi.org/10.1289/ehp.1409481.

Martins, H., 2012. Urban compaction or dispersion? An air quality modelling study. Atmos. Environ. 54, 60–72, http://dx.doi.org/10.1016/j.atmosenv.2012.02.075.

McGarigal, K., Cushman, S.A., Ene, E., 2012. FRAGSTATS v4: Spatial Pattern Analysis Program for Categorical and Continuous Maps. Computer software program produced by the authors at the University of Massachusetts, Amherst.

Pant, P., Guttikunda, S.K., Peltier, R.E., 2016. Exposure to particulate matter in India: a synthesis of findings and future directions. Environ. Res. 147, 480–496, http://dx.doi.org/10.1016/j.envres.2016.03.011.

Pardyjak, E.R., Fernando, H., Joseph, S., Hunt, J.C.R.G., Anderson, J., 2009. A case study of the development of nocturnal slope flows in a wide open valley and associated air quality implications. Meteo Z. 18, 85–100, http://dx.doi.org/10.1127/0941-2948/2009/362.

Phung, D., Hien, T.T., Linh, H.N., Luong, L.M.T., Morawska, L., Chu, C., Binh, N.D., Thai, P.K., 2016. Air pollution and risk of respiratory and cardiovascular hospitalizations in the most populous city in Vietnam. Sci. Total Environ. 557–558, 322–330, http://dx.doi.org/10.1016/j.scitotenv.2016.03.070.

Pope, C.A., Dockery, D.W., 2006. Health effects of fine particulate air pollution: lines that connect. J. Air Waste Manage. Assoc. 56, 709–742, http://dx.doi.org/10.1080/10473289.2006.10464545.

Pope, R., Wu, J., 2014a. Characterizing air pollution patterns on multiple time scales in urban areas: a landscape ecological approach. Urban Ecosyst. 17, 855–874, http://dx.doi.org/10.1007/s11252-014-0357-0.

Pope, R., Wu, J., 2014b. A multi-objective assessment of an air quality monitoring network using environmental, economic, and social indicators and GIS-based models. J. Air Waste Manage. Assoc. 64, 721–737, http://dx.doi.org/10.1080/10962247.2014.888378.

Rolph, G.D., 2016. Real-time Environmental Applications and Display System (READY) Website (http://www.ready.noaa.gov). NOAA Air Resources Laboratory, College Park, MD.

Schwartz, J., Dockery, D.W., Neas, L.M., 1996. Is daily mortality associated specifically with fine particles? J. Air Waste Manage. Assoc. 46, 927–939, http://dx.doi.org/10.1080/10473289.1996.10467528.

Shao, M., Tang, X., Zhang, Y., Li, W., 2006. City clusters in China: air and surface water pollution. Front. Ecol. Environ. 4, 353–361, http://dx.doi.org/10.1890/1540-9295(2006)004[0353:ccicaa]2.0.co;2.

Shi, T., Liu, Y., Zhang, L., Hao, L., Gao, Z., 2014. Burning in agricultural landscapes: an emerging natural and human issue in China. Landsc. Ecol. 29, 1785–1798, http://dx.doi.org/10.1007/s10980-014-0060-9.

Stein, A.F., Draxler, R.R., Rolph, G.D., Stunder, B.J.B., Cohen, M.D., Ngan, F., 2015. NOAA's HYSPLIT atmospheric transport and dispersion modeling system. Bull. Am. Meteorol. Soc. 96, 2059–2077, http://dx.doi.org/10.1175/BAMS-D-14-00110.1.

Tao, M., Chen, L., Su, L., Tao, J., 2012. Satellite observation of regional haze pollution over the North China Plain. J. Geogr. Sci. Atmos. 117, http://dx.doi.org/10.1029/2012jd017915, D12203.

Tao, M., Chen, L., Wang, Z., Ma, P., Tao, J., Jia, S., 2014. A study of urban pollution and haze clouds over northern China during the dusty season based on satellite and surface observations. Atmos. Environ. 82, 183–192, http://dx.doi.org/10.1016/j.atmosenv.2013.10.010.

Tsangari, H., Paschalidou, A.K., Kassomenos, A.P., Vardoulakis, S., Heaviside, C., Georgiou, K.E., Yamasaki, E.N., 2016. Extreme weather and air pollution effects on cardiovascular and respiratory hospital admissions in Cyprus. Sci. Total Environ. 542 (Part A), 247–253, http://dx.doi.org/10.1016/j.scitotenv.2015.10.106.

World Health Organization (WHO), 2005. Air Quality Guidelines: Global Update 2005. World Health Organization.

Wang, J., Christopher, S.A., 2003. Intercomparison between satellite-derived aerosol optical thickness and PM2.5 mass: implications for air quality studies. Geogr. Res. Lett. 30 (2095), http://dx.doi.org/10.1029/2003gl018174.

Wang, X., Liang, X., Jiang, W., Tao, Z., Wang, J.X.L., Liu, H., Han, Z., Liu, S., Zhang, Y., Grell, G.A., Peckham, S.E., 2010a. WRF-chem simulation of East Asian air quality: sensitivity to temporal and vertical emissions distributions. Atmos. Environ. 44, 660–669, http://dx.doi.org/10.1016/j.atmosenv.2009.11.011.

Wang, Z., Chen, L., Tao, J., Zhang, Y., Su, L., 2010b. Satellite-based estimation of regional particulate matter (PM) in Beijing using vertical-and-RH correcting method. Remote Sens. Environ. 114, 50–63, http://dx.doi.org/10.1016/j.rse.2009.08.009.

Wang, L., Xu, J., Yang, J., Zhao, X., Wei, W., Cheng, D., Pan, X., Su, J., 2012a. Understanding haze pollution over the southern Hebei area of China using the CMAQ model. Atmos. Environ. 56, 69–79, http://dx.doi.org/10.1016/j.atmosenv.2012.04.013.

Wang, T., Jiang, F., Deng, J., Shen, Y., Fu, Q., Wang, Q., Fu, Y., Xu, J., Zhang, D., 2012b. Urban air quality and regional haze weather forecast for Yangtze River Delta region. Atmos. Environ. 58, 70–83, http://dx.doi.org/10.1016/j.atmosenv.2012.01.014.

Wang, H., Tan, S., Wang, Y., Jiang, C., Shi, G., Zhang, M., Che, H., 2014. A multisource observation study of the severe prolonged regional haze episode over eastern China in January 2013. Atmos. Environ. 89, 807–815, http://dx.doi.org/10.1016/j.atmosenv.2014.03.004.

Wu, J., Shen, W., Sun, W., Tueller, P.T., 2002. Empirical patterns of the effects of changing scale on landscape metrics. Landsc. Ecol. 17, 761–782, http://dx.doi.org/10.1023/a:1022995922992.

Wu, J., Jenerette, G.D., Buyantuyev, A., Redman, C.L., 2011. Quantifying spatiotemporal patterns of urbanization: the case of the two fastest growing metropolitan regions in the United States. Ecol. Complex 8, 1–8, http://dx.doi.org/10.1016/j.ecocom.2010.03.002.

Wu, J., Xiang, W., Zhao, J., 2014. Urban ecology in China: historical developments and future directions. Landsc. Urban Plan. 125, 222–233, http://dx.doi.org/10.1016/j.landurbplan.2014.02.010.

Wu, J., 1999. Hierarchy and scaling: extrapolating information along a scaling ladder. Can. J. Remote Sens. 25, 367–380, http://dx.doi.org/10.1080/07038992.1999.10874736.

Wu, J., 2004. Effects of changing scale on landscape pattern analysis: scaling relations. Landsc. Ecol. 19, 125–138, http://dx.doi.org/10.1023/B:LAND.0000021711.40074. ae.

van Donkelaar, A., Martin, R.V., Park, R.J., 2006. Estimating ground-level PM2.5 using aerosol optical depth determined from satellite remote sensing. J. Geogr. Sci. Atmos. 111, http://dx.doi.org/10.1029/2005jd006996, D21201.

van Donkelaar, A., Martin, R.V., Brauer, M., Kahn, R., Levy, R., Verduzco, C., Villeneuve, P.J., 2010. Global estimates of ambient fine particulate matter concentrations from satellite-based aerosol optical depth: development and application. Environ. Health. Persp. 118, 847–855, http://dx.doi.org/10.1289/ehp.090l62.

van Donkelaar, A., Martin, R.V., Brauer, M., Boys, B.L., 2015. Use of satellite observations for long-term exposure assessment of global concentrations of fine particulate matter. Environ. Health. Persp. 123, 135–143, http://dx.doi.org/10.1289/ehp.1408646.

Xu, B., Luo, L., Lin, B., 2016. A dynamic analysis of air pollution emissions in China: evidence from nonparametric additive regression models. Ecol. Indic. 63, 346–358, http://dx.doi.org/10.1016/j.ecolind.2015.11.012.

Yahya, K., Zhang, Y., Vukovich, J.M., 2014. Real-time air quality forecasting over the southeastern United States using WRF/Chem-MADRID: multiple-year assessment and sensitivity studies. Atmos. Environ. 92, 318–338, http://dx.doi.org/10.1016/j.atmosenv.2014.04.024.

Yuan, Q., Yang, L., Dong, C., Yan, C., Meng, C., Sui, X., Wang, W., 2014. Temporal variations, acidity, and transport patterns of PM2.5 ionic components at a background site in the Yellow River Delta, China. Air Qual. Atmos. Health. 7, 143–153, http://dx.doi.org/10.1007/s11869-014-0236-0.

Zhang, X.Y., Wang, Y.Q., Lin, W.L., Zhang, Y.M., Zhang, X.C., Zhao, P., Yang, Y.Q., Wang, J.Z., Hou, Q., Che, H.Z., Guo, J.P., Li, Y., Gong, S., Zhang, X.L., 2009. Changes of atmospheric composition and optical properties over Beijing–2008 Olympic Monitoring Campaign. Bull. Am. Meteorol. Soc. 90, 1633–1651, http://dx.doi.org/10.1175/2009bams2804.1.

Zhang, X.X., Shi, P.J., Liu, L.Y., Tang, Y., Cao, H.W., Zhang, X.N., Hu, X., Guo, L.L., Lue, Y.L., Qu, Z.Q., Jia, Z.J., Yang, Y.Y., 2010. Ambient TSP concentration and dustfall in major cities of China: spatial distribution and temporal variability. Atmos. Environ. 44, 1641–1648, http://dx.doi.org/10.1016/j.atmosenv.2010.01.035.